# Hollow Graphitic Carbon Nanospheres Synthesized by Rapid Pyrolytic Carbonization

Cheng Zhang<sup>1,a\*</sup>, Qingshan Gao<sup>2,b</sup>, Luyun Jiao<sup>1,c</sup>, Laura Bogen<sup>1,d</sup>, Nicole Forte<sup>1,e</sup> and Elizabeth Nestler<sup>1,f</sup>

<sup>1</sup>Department of Chemistry, Long Island University (Post), Brookville, NY 11548, USA
<sup>2</sup>School of Applied Chemistry and Bioengineering, Weifang Engineering Vocational College, Qingzhou, Shandong 262500, China

#### Email:

<sup>a</sup>cheng.zhang@liu.edu, <sup>b</sup>gaocarbon@gmail.com,

°luyun.jiao@my.liu.edu, <sup>d</sup>laura.bogen@my.liu.edu
enicole.forte2@my.liu.edu, <sup>f</sup>Elizabeth.nestler@my.liu.edu

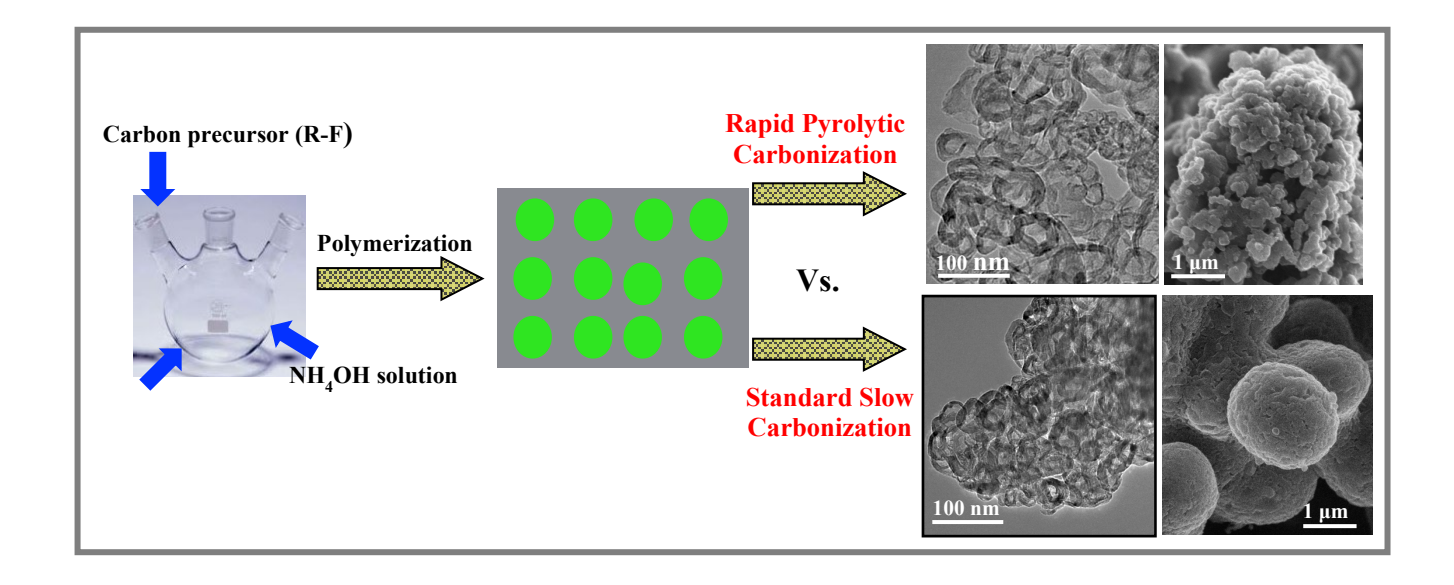
\*Address all correspondence to this author.

#### **Abstract**

Hollow graphitic porous carbon nanosphere (CNS) materials are synthesized from polymerization of resorcinol (R) and formaldehyde (F) in the presence of templating iron polymeric complex (IPC), followed by carbonization treatment. The effect of rapid heating in the carbonization process is investigated for the formation of hollow graphitic carbon nanospheres. The resulting CNS from rapid heating was characterized for its structure and properties by transmission electron microscope (TEM), x-ray diffraction (XRD), Raman spectroscopy, bulk conductivity measurement and Brunauer-Emmett-Teller (BET) surface area. Hollow graphitic CNS with reduced degree of agglomeration is observed under rapid heating during the carbonization process when compared to the CNS synthesized using the standard slow heating approach.

Key words: carbon nanosphere (CNS), rapid pyrolytic carbonization, agglomeration

# **Graphical Abstract**



#### 1. Introduction

Carbon is one of the most abundant elements on earth with many natural structures such as soot, diamond and graphite [1]. Carbon-based materials have been used for a wide variety of applications [2-3]. In general, graphitic carbon is preferred over amorphous carbon due to the desirable properties associated with graphitic carbon, such as well-defined crystalline structure, high electric conductivity, decent thermal stability, and reasonable oxidation resistance at low temperature [4]. Over the past three decades, several breakthroughs have been witnessed in carbon research for the discoveries of fullerenes [5], graphene [6] and nanotubes [3]. There have been enormous interests in the fabrication of new carbon-based nanomaterials with highly curved graphitic structures [7]. Tremendous efforts to tune the shape and size of carbon nanomaterials during the growth process have been put forth in the synthesis of a wide variety of carbon nanomaterials in the form of nanocages [8,9], nano onions [10], nanoflakes [11], nanoplates [12], nanorods [13], nanoballs [14], and nanospheres [1,15-21]. Among all these nanostructured materials, carbon nanospheres (CNS) have a number of potential applications in energy storage and conversion [22,23], catalysis [24,25], drug delivery [26], optoelectronics [18], solid lubricants [27], and composite materials [28]. Some recent work reported the application of various carbon forms in nanocomposites [29-37].

Reported methods for CNS synthesis include chemical vapor deposition [38], arc discharge [39], acetylene flaming [40], laser pyrolysis [41], NaCl templating [42], catalytic-reduction [43], solvo-chemical approach [44], pyrolysis of ferrocene [45], silica templating [38,46], and others. We previously reported the synthesis of hollow graphitic CNS, with inner diameter of 20–50 nm and shell thickness of 10–15 nm, from a carbon rich precursor (IPC) using iron nanoparticles as template and catalyst [15,16]. The uniform and narrow particle size (<3 nm) of the IPC ensures reproducible synthesis of uniform CNS with unique properties [15]. One of the major challenges in the synthesis of CNS is the agglomeration in the nano-scale. Although different methods have been investigated to reduce the agglomeration [47-50], the issue remains an obstacle for the preparation of high-fidelity nanoparticles.

In the past decades, rapid thermal treatments such as microwave irradiation [51,52], rapid thermal shock method [53], fast pyrolysis [54], and rapid thermal annealing [55], have emerged as powerful tools for the synthesis and functionalization of carbon nanomaterials with less agglomeration. For example, Yao et.al. reported that the rapid thermal shock method offered considerable potential for the bulk synthesis of un-agglomerated nanoparticles stabilized within a matrix [56]. In our earlier work, CNS materials were synthesized by typical slow heating of carbonization process [15,16]. Agglomeration of CNS has been observed in the prepared materials. We hypothesize that the slow heating rate in the process may have caused the steady fusion and annealing between the external walls of the particles, resulting the agglomerated CNS. In this work, we investigated the effect of rapid heating process on the structure and properties of the synthesized CNS. The carbon precursor in a quartz tube was pushed to the center of the furnace at 1000°C within 10 seconds; the tube was kept in the furnace for different duration. To the best of our knowledge, this approach (rapid pyrolytic carbonization) is the first demonstration to obtain hollow graphitic CNS with reduced degree of agglomeration. The novelty of this work will facilitate the fabrication of less agglomerated materials thus lead to a wide applications of such materials in nanocomposite and catalysis. Furthermore, high graphitic content is an important property for the CNS in the application of batteries. To obtain ordered graphitic structure, the synthesized CNSs were then annealed in a vacuum furnace at different temperatures of 1400°C~2000°C for a period of 2 hours each. Raman, bulk conductivity and BET surface area were conducted for the annealed CNS.

#### 2. Materials and Methods

#### 2.1 Material

Resorcinol, formaldehyde (37% in water) citric acid, and ammonium hydroxide (28% in water) were purchased from Sigma-Aldrich and used without further treatment; Iron powder (100 mesh) was purchased from Spectrum; nitric acid and chloric acid were purchased from Fisher Chemicals.

#### 2.2 Synthesis of CNS-rpc

The synthesis of CNS was modified based on our previously reported work [25,26,52]. The synthesized CNS from this rapid pyrolytic carbonization is denoted as CNS-*rpc*. The detailed procedure was described as follows:

**Synthesis of iron polymeric complex (IPC) (iron precursor)** A 0.1 M iron precursor solution was prepared using 2.8 g of iron powder, 9.6 g of citric acid in 1:1 molar ratio, and 0.50 L of water. The above mixture was vigorously stirred in the open air in a 1.0 L beaker. After 24 hours, a clear greenish-vellow solution was obtained and filtered for the CNS synthesis.

**Polymerization** 18.0 g of formaldehyde (37% in water), 12.20 g of resorcinol, and 200 ml of above synthesized IPC solution (0.1M) were placed to a round bottom three-neck flask. The solution was agitated until resorcinol was completely dissolved. 20 ml of NH4OH was subsequently added dropwise with strong mechanical stirring. The pH of the above mixture reached to about 10 and then aged at 90 °C for 3 hours. The synthesized polymer was collected by filtration and dried at 70°C in an oven for 5 hours.

**Rapid pyrolytic carbonization (RPC) or rapid heating** 1.5 g of the above synthesized polymer was placed in a quartz tube, which was pushed to the center of the furnace at 1000 °C within 10 seconds; the tube was kept in the furnace for 0.5 hour, 1 hour, and 2 hours, respectively. N<sub>2</sub> was purged through the chamber during the carbonization process.

**Purification** The above carbonized product was refluxed in nitric acid (5 M) for 2 hours, followed by refluxing in hydrochloric acid (4 M) for 2 hours. The above product was washed with plenty amount of water until the pH reached to neutral. The final product was collected and dried at 80 °C for 5 hour in an oven.

The CNS synthesized from this rapid pyrolytic carbonization at various duration is denoted as CNSrpc-0.5h, CNS-rpc-1h and CNS-rpc-2h, respectively. CNS-rpc-2h was further annealed in a vacuum furnace at different temperatures of 1400 °C, 1600 °C, 1800 °C and 2000 °C for a period of 2 hours each, which were conducted on Raman, bulk conductivity and BET surface area studies. Those annealed samples are denoted as CNS-ann-1400, CNS-ann-1600, CNS-ann-1800 and CNS-ann-2000, respectively.

#### 2.3 CNS characterization

Specimens for Transmission Electron Microscopy (TEM) were prepared by dispersing the powdered samples in isopropanol for 30 minutes in the ultrasonic bath. A droplet of the colloidal suspension was then placed onto a Cu grid with a porous carbon film, followed by drying in air. The samples were scanned by a TEM/STEM (JEOL 2010F) operated at 200 KV.

JEOL 7500F Field-Emission Gun High-Resolution Scanning Electron Microscopy (SEM) was used for SEM measurement at 1-4 kV. Samples in powdered form were clung to aluminum stubs with carbon tape. To squander the effects of charging, "gentle beam" mode was used for imaging the samples, where the phase is subjective to below the accelerating voltage of the microscope.

Raman analysis was carried out using a Renishaw 1000/2000 spectrometer using back-scattering geometry under an excitation wavelength of 514 nm<sup>-1</sup>. A 50x objective was utilized with 10% laser power and an exposure time of 60 s for static scans and 100 s for extended scans, and 2 accumulations per scan were collected.

Surface area and pore volume analysis of the powdered samples were conducted using Micromeritics Tristar Surface Area and Porosity Analyzer. Nitrogen gas was used as the adsorbate. Analysis was carried out at -196°C after 300°C overnight out-gassing. The surface area was determined by the Brunauer-Emmett-Teller (BET) method.

The bulk electrical conductivity measurement was conducted in a cell containing a quartz capillary (0.15 cm diameter and 10 cm length) with two copper electrodes connected to a voltage/current source (Keithley 228A). The copper electrodes were used to compress and position the sample powder in the capillary tube.

#### 3. Results and Discussion

#### 3.1 Synthesis of CNS-rpc

As reported previously, the standard method to synthesize CNS was started with an iron precursor (IPC) as a template and dispersant during the polymerization process of resorcinol and formaldehyde, followed by standard carbonization and purification process [15,16]. The typical carbonization process was carried out under the temperature program as follows: heat to 1000 °C at 20 °C/min, hold at 1000 °C for 5 h, and cool to room temperature under N<sub>2</sub> atmosphere. Using the standard method, hollow graphitic CNS was synthesized but accompanied with severe agglomeration. The agglomeration would limit the usage of this type of CNS for a wide range of applications in catalyst support, polymer composite as filler, absorbent, anion electrode, electric capacitor, and many more [22-27,49]. It is hypothesized that rapid pyrolytic carbonization may accelerate the CNS formation by rapid carbon deposition onto the surface of iron nanoparticles by having the polymer precursor RF-Fe(OH)<sub>3</sub> subjected to high temperature in a short period of time before the iron particles could fuse and agglomerate. For this purpose, we designed a series of experiments by rapidly heating the sample in N<sub>2</sub> atmosphere from room temperature to 1000 °C within 10 seconds and kept at 1000 °C for 30 min, 1 hour, and 2 hours, respectively. The modified synthetic procedure for CNS consists of three steps as shown in Fig. 1: (1) polymerization process of formaldehyde (F) and resorcinaol (R) in the presence of homogeneously distributed IPC by slow addition of ammonium hydroxide to reach pH = 10. In this process, the crystal structure and the transmisstion electron micrographs of IPC as displayed in Fig. 1 were reported in our previous work [15,16]; (2) rapid carbonization process of produced R-F polymers containing enclosed iron: the R-F polymer enclosed iron was slided to the center of the furnace at 1000 °C within 10 seconds and kept for a required duaration. N2 was purged through the chamber during the carbonization process; and (3) purification process to eliminate iron and amorphous carbon to obtain holllow graphitic CNS [15]. In this work, we investigated how the rapid carbonization process improved the structure and property of the resulting materials.

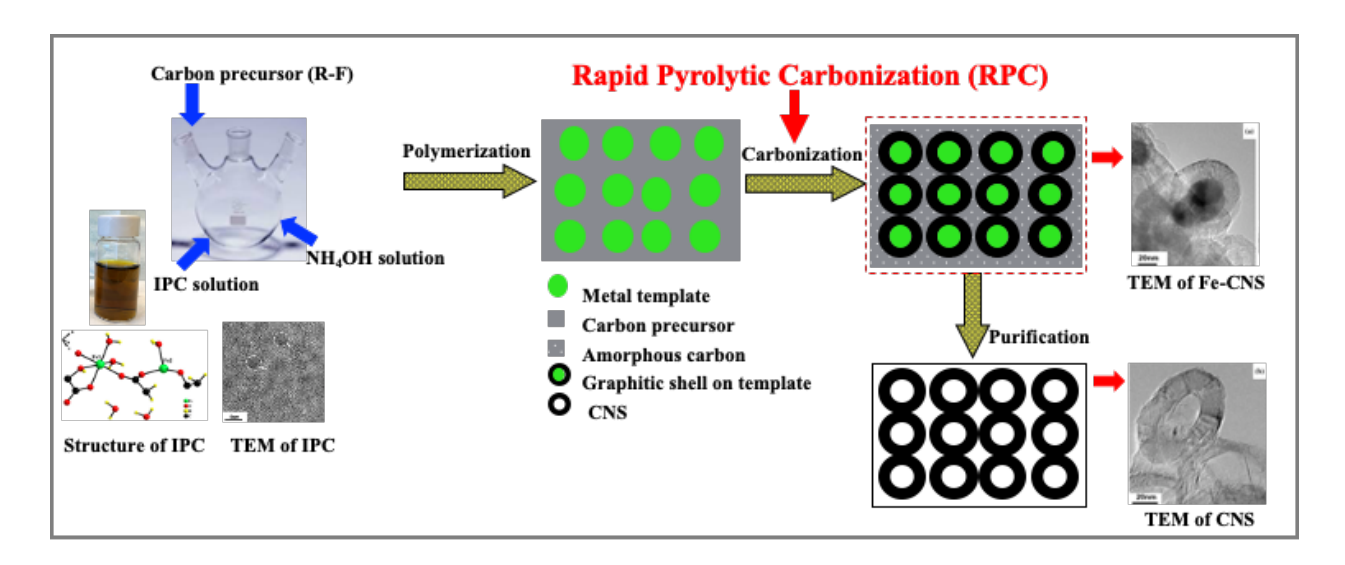
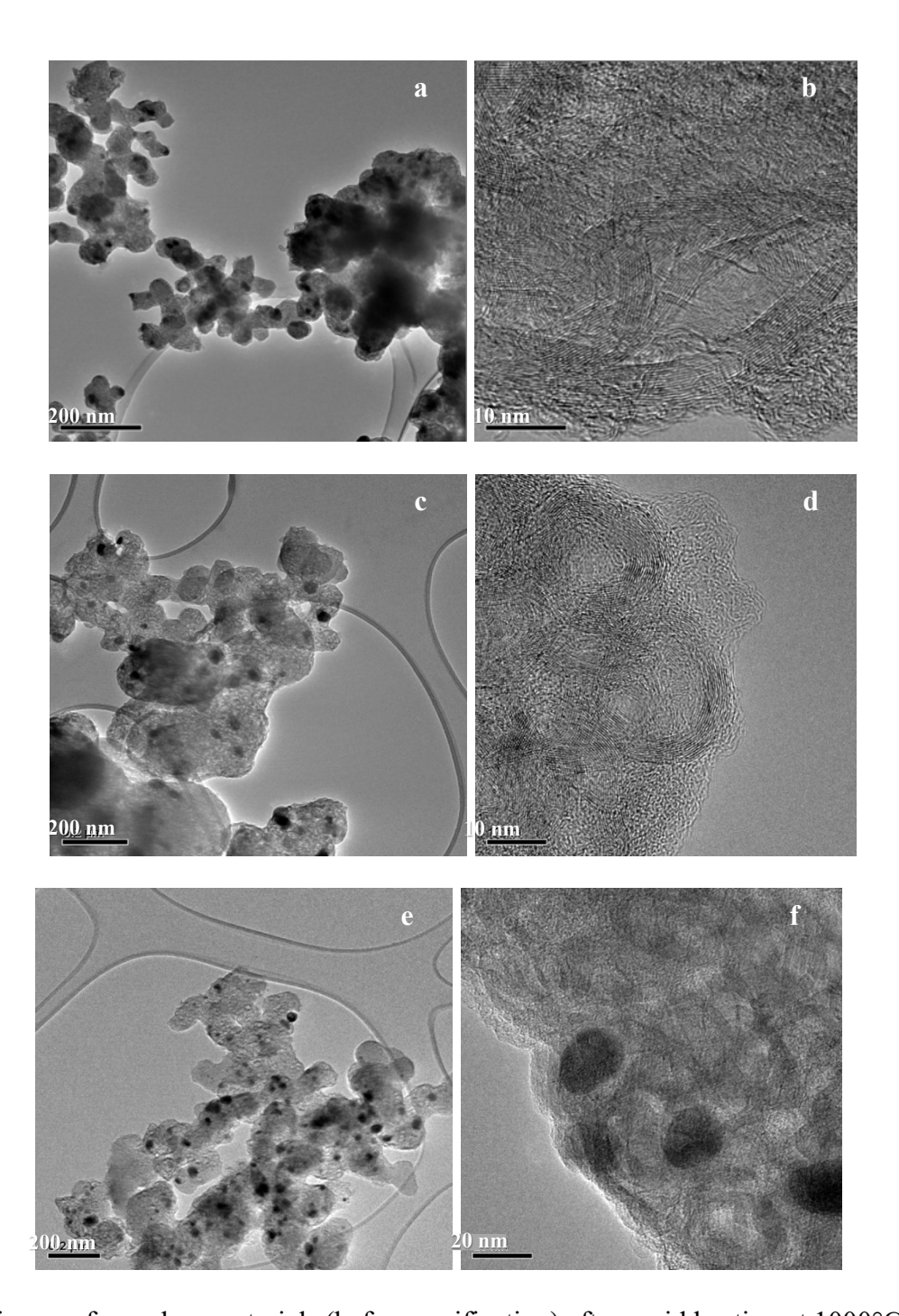


Figure 1: CNS Synthetic Process

## 3.2 Characterization of CNS-rpc

#### 3.2.1 TEM and XRD

TEM images for the carbon product after the rapid carbonization process (before purification) at 1000 °C for 30 minutes, 1 hour and 2 hours are shown in Figure 2 (a-f). Figure 2 (a, b) clearly shows the graphitic structures along with large Fe nanoparticles. Convoluted spheres were observed due to insufficient time to form distinct spheres. After being kept at 1000 °C for 1 hour, more graphitic structures and distinct spheres were formed (Figure 2, c and d). And after carbonization for 2 hours, even more graphitic structures and distinct spheres are observed (Figure 2, e and f). Compared to the slow heating process in the previous work [15], which produced round shapes with even edges, the rapid heating process in this work caused the formation of ginger-root shaped structures which is probably due to the sudden pyrolytic fragmentation of the cross-linked polymer as a result of the rapid increase of the temperature. This unique ginger-root shaped material may have unique mechanical reinforcement properties.



**Figure 2:** TEM images for carbon materials (before purification) after rapid heating at 1000°C for 30 minutes (a, b); for 1 hour (c, d); for 2 hours (e, f).

The XRD patterns of polymers before and after rapid heating at 1000 °C for 30 min are depicted in Figure 3 (a) and (b). Before carbonization, a broad peak is observed and ascribed to an amorphous structure. After rapid heating at 1000 °C, the structure is transformed to increased crystallinity. The sharp peak at  $2\theta = 26^{\circ}$  was ascribed to the graphite peak of (002). The (100) peak at  $2\theta$  of about 42.4

and (101) peak at about 43.7 provided additional confirmation on the formation of graphitic structure. The broad diffraction base of the (002), (100) and (101) peaks suggested a limited amount of disordered carbon still remained after rapid heating at 1000°C for 30 minutes. The sharp peaks at 20 = 44.6, 65.1 are ascribed to the (110) and (200) reflection of Fe (FCC). Several other crystalline iron species such as Fe<sub>3</sub>C, Fe<sub>3</sub>O<sub>4</sub>, and Fe (BCC) were also detected by XRD.

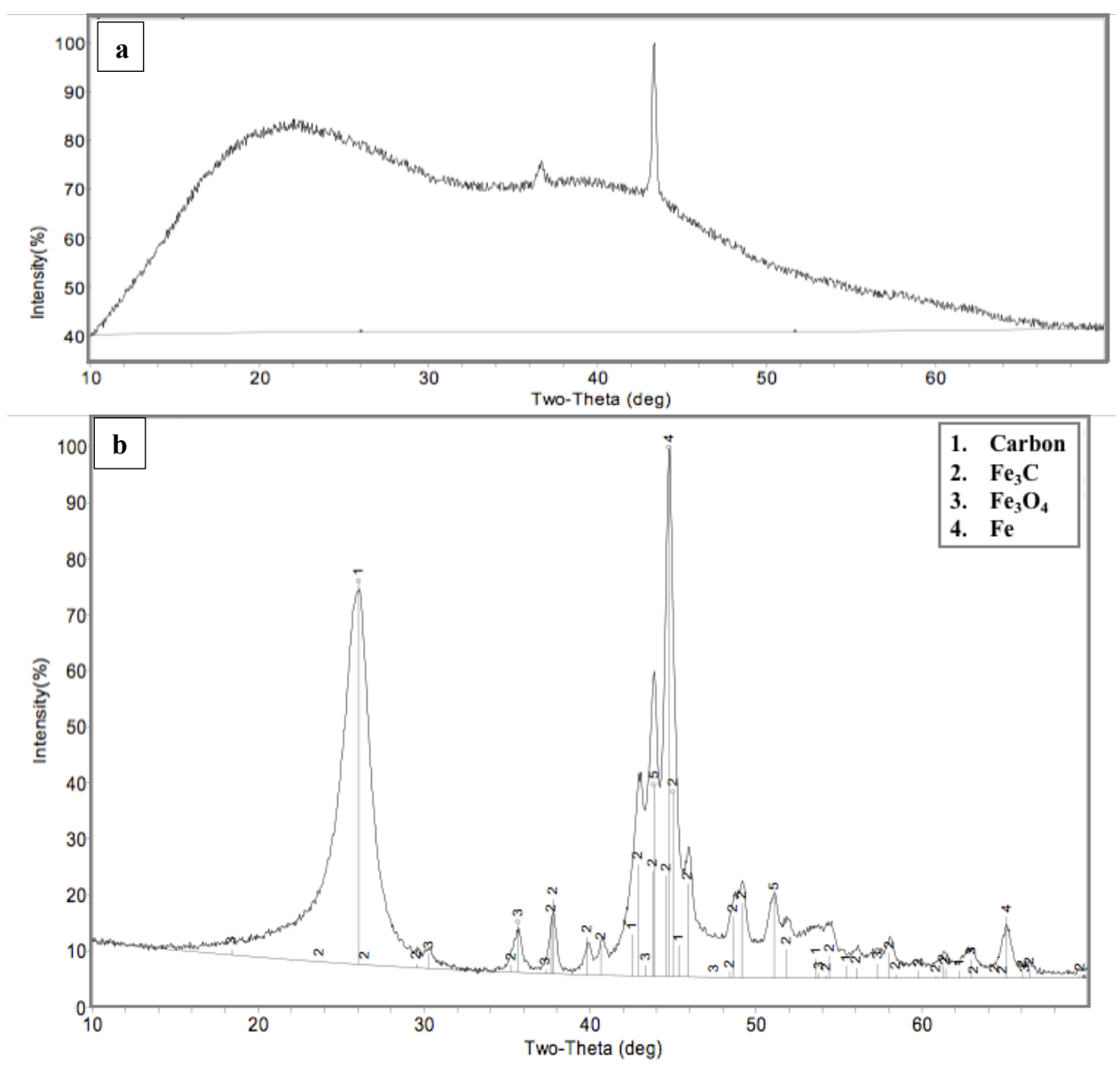


**Figure 3:** XRD patterns of polymer (a) before and (b) after rapid heating and kept at 1000°C for 30 minutes

After the purification process in 5 M nitric acid for two hours and 4 M hydrochloric acid for two hours, the majority of amorphous carbon and iron were removed and graphitic carbon nanospheres at < 50 nm were observed as shown in Figure 4a and b. For direct comparison, the CNS produced using the standard slow carbonization process are shown in Figure 4c and d. The TEM imagies clearly show that the CNS synthesized by the rapid heating process displays reduced degree of agglomeration when compare to the CNS synthesized using the standard approach. The reduced degree of agglomeration is consistent with our hypothesis on the rapid deposition of carbon onto the surface of less agglomerated iron nanoparticles when the polymer precursor enclosed iron core was rapidly subjected to high temperature carbonization (within 10 second). Moreover, it appears that less uniform CNS particle size was formed for the synthesized CNS-*rpc*-2h with some portion of smaller particle size (~20 nm) as evidenced in Figure 4a. Yao et al. reported that rapid thermal shock enabled the formation of smaller sizes of nanoparticles with less agglomeration within a matrix [56].

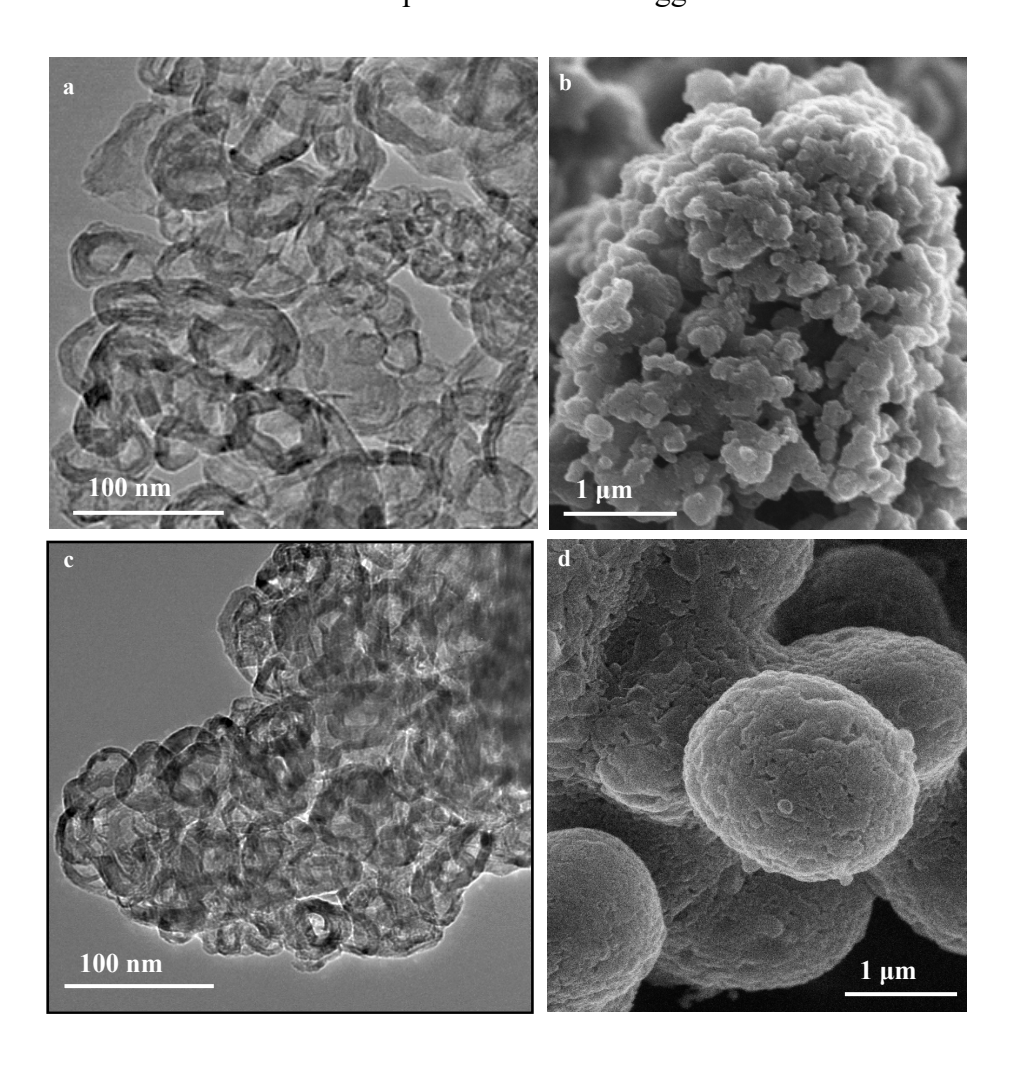


**Figure 4:** a) TEM and b) SEM images for CNS product after rapid heating at 1000°C for 2 hours (CNS-*rpc*-2h); c) TEM and d) SEM images for CNS product after standard slow carbonization

#### **3.2.2 Raman**

High graphitic content is an important property for CNS as anode materials for Li-ion batteries [23,57]. We employed Raman spectroscopy to further characterize the synthesized materials. The purpose of annealing the samples is to obtain well-ordered graphitic structure so as to further improve the graphitic content. The CNS-*rpc*-2h was selected for further annealing as it exhibited more graphitic and distinct spheres after carbonization for 2 hours (Figure 5). Annealing of the CNS-*rpc*-2h was carried out in a vacuum furnace at different temperatures of 1400 °C, 1600 °C, 1800 °C and 2000 °C for a period of 2 hours each. Those annealed samples are denoted as CNS-*ann*-1400, CNS-*ann*-1600, CNS-*ann*-1800 and CNS-*ann*-2000, respectively. The spectra for those annealed samples are compared with the raw CNS sample (CNS-*rpc*-2h, before annealing) in Figures 5. The major features of the Raman spectra could be seen at about 1354 cm<sup>-1</sup>, 1581 cm<sup>-1</sup> and 2700 cm<sup>-1</sup>, namely the D (disorder carbon peak), G (graphite carbon peak) and G' (2D) peaks. Minor peaks at 2450 cm<sup>-1</sup>, 2950 cm<sup>-1</sup> and 3242 cm<sup>-1</sup> made up the second order region. All these features are present in the five samples and show minimal variations.

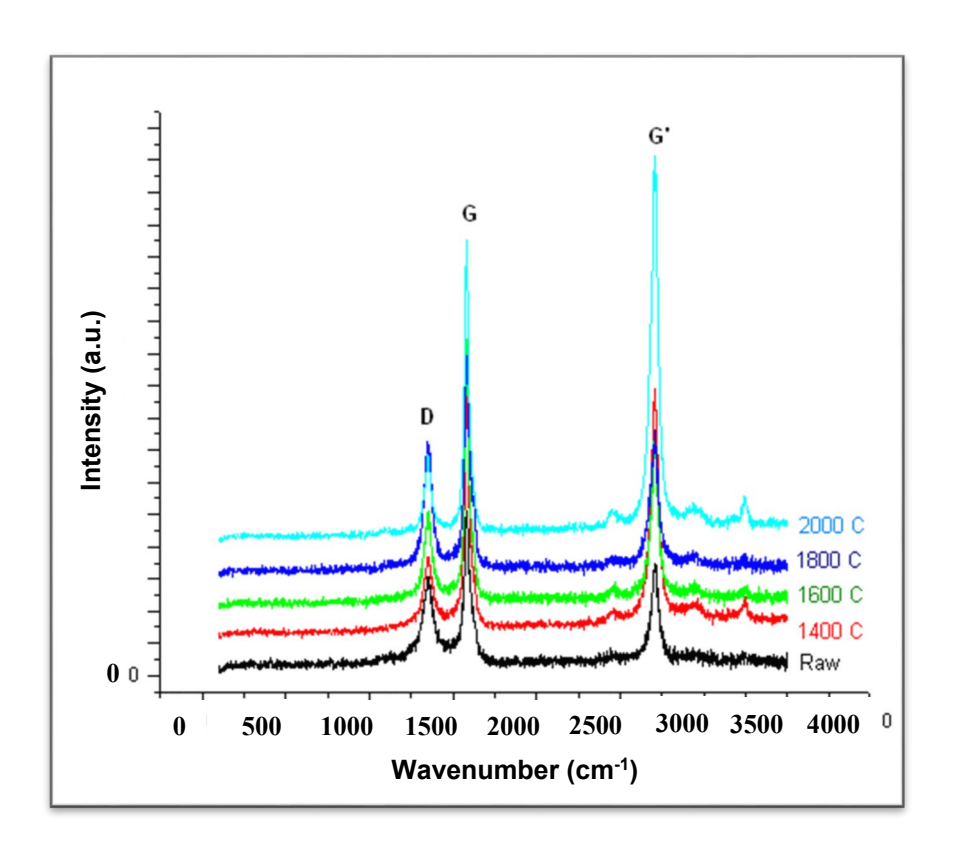


**Figure 5:** Raman Spectra of CNS-*rpc*-2h (raw) and the annealed samples CNS-*ann*-1400 (1400 °C), CNS-*ann*-1600 (1600 °C), CNS-*ann*-1800 (1800 °C) and CNS-*ann*-2000 (2000 °C)

Figure 5 shows that the synthesized CNS-*rpc* after purification process was already highly graphitic and ordered. The effect of annealing on the CNS-*rpc*-2h (raw sample) was weakly pronounced. The D band changed to a certain extent, which suggested no major structural changes. It could be inferred that the graphitic layers became more ordered upon annealing, as the D band reduced in height and the G band increased in height. A sharp increase in height for the G band was observed when temperature was increased from 1800 °C to 2000 °C.

We further calculated the Full Width at Half Maximum (FWHM) of the D and G bands observed in Raman spectra. FWHM is the average width of the peaks and corresponds to the uniform homogeneity of Raman active species. Table 1 shows the FWHM of the samples. Annealing induces a general reduction in the FWHM values for D band, indicating narrowing of the peaks and thus increased graphitic structural ordering. However, a marginal increase was observed in the G band's FWHM for the sample annealed at 1600 °C, including a broadening of the D band. This result together

with the appearance of a shoulder at around 1620 cm<sup>-1</sup> indicated the initiation of change in the shell structure. This band at 1620 cm<sup>-1</sup> was associated with a defect provoked carbon (sp<sup>2</sup>) that does not have in-plane symmetry [50,58]. The shoulder, nonetheless diminishes on further annealing, is reflected by the FWHM values of the samples annealed at 1800 °C and 2000 °C. A significant decrease in FWHM for the G band is observed at 2000 °C.

**Table 1.** FWHM of the synthesized CNS-*rpc*-2h annealed at 1400~2000°C

FWHM (cm <sup>-1</sup> )	D Band	G Band
CNS-rpc-2h (raw)	124	48
CNS-ann-1400 (1400°C)	76	44
CNS-ann-1600 (1600°C)	115	61
CNS-ann-1800 (1800°C)	68	53
CNS-ann-2000 (2000°C)	57	37

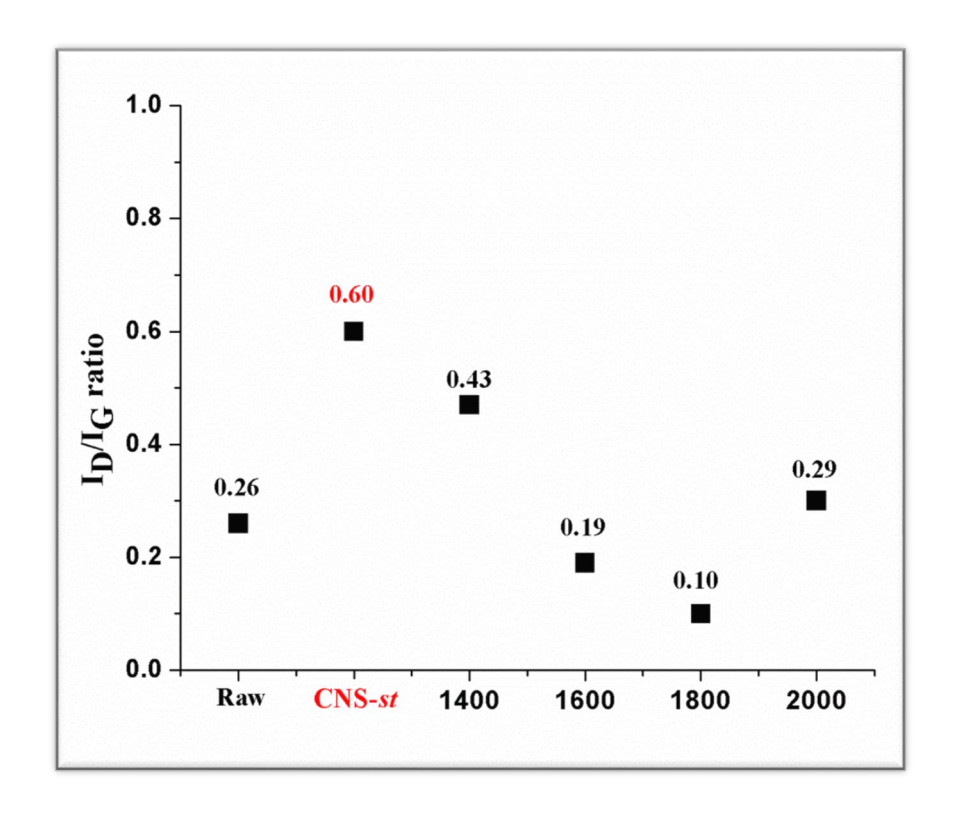


**Figure 6:**  $I_D/I_G$  ratio of the synthesized CNS-rpc-2h (raw) annealed at temperatures of  $1400\sim2000^{\circ}$ C to compare with CNS-st

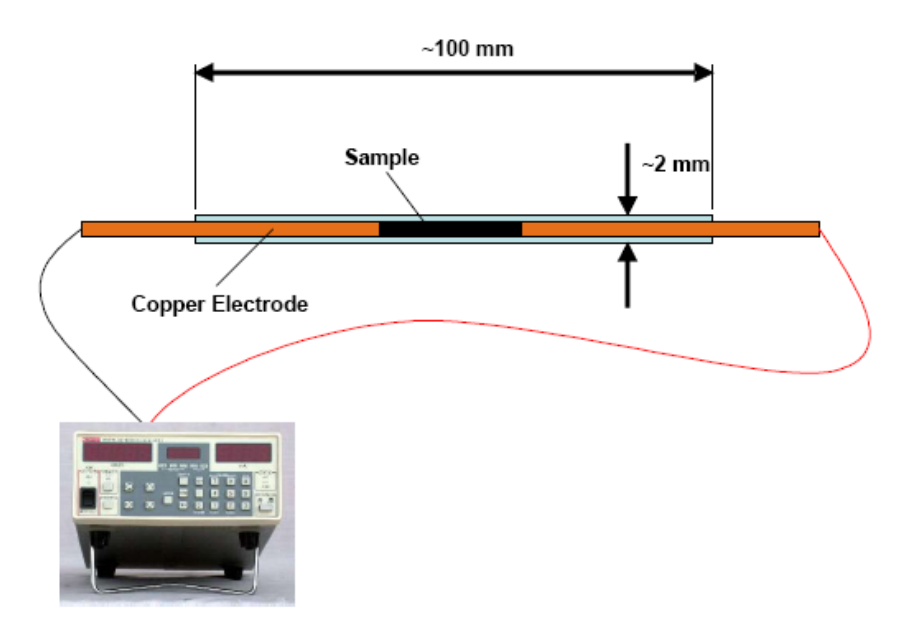
The ratios of peak areas of disorder peak (D) to graphite peak (G) were also calculated, by normalizing the spectra using the maximum intensity value in each spectrum and then baseline corrected using automatic positive peak algorithm for two points [59]. The relative intensity ratio of

In and IG for the D and G band is regarded as the typical quantity for the content of graphitization: the greater the ratio of ID/IG, the higher the disorder content for graphite [59]. As shown in Figure 6, a plot of the ID/IG for the synthesized CNS-rpc-2h and the annealed samples are compared with that for the CNS-st synthesized using the standard carbonization process. It can be seen that, for the ratios for CNS-rpc-2h and the annealed samples , the ID/IG ratios are in the range of 0.1 to 0.5. Strains due to bending of graphite shells upon annealing rather than increased disorder induce some increase in the ID/IG after annealing at 1400 °C (0.43) and 2000 °C (0.29). However, the ratio of ID/IG for the synthesized CNS-rpc-2h and the annealed samples are all smaller than that for CNS-st (0.60) in the previous work [15], reflecting the higher degree of graphitization of the CNS-rpc-2h and the annealed samples at 1400~2000 °C in this work. The results further show that the synthesized CNS-rpc-2h after the purification process is sufficiently graphitized. Annealing the CNS-rpc-2h in the temperature range of 1400 °C to 2000 °C does not affect its graphitic nature to any significant extent. The slightly increased ID/IG for the CNS-rpc-2h annealed at 2000 °C is probably due to the certain degree collapse of the CNS structure.

#### 3.2.3 Bulk Conductivity

The CNS-*rpc*-2h and the annealed samples at 1400 °C, 1600 °C, 1800 °C and 2000 °C, respectively, were measured for electrical conductivity using a four-point probe resistance measurement setup as reported in the previous publications [15,16]. An Arkema multiwalled carbon nanotube sample was measured as a reference in comparison with the CNS-*rpc*-2h and the annealed samples. Table 2 and Figure 7 show the relative resistance values for each sample. Resistance is related to resistivity; the lower the resistivity, the more conductive is the material. Conductivity is one of the important properties for carbon-based material. The bulk conductivity of the synthesized CNS-*rpc*-2h and the annealed samples were measured using a setup as shown in Scheme 1. The measurement cell consisted of a quartz capillary and two copper electrodes, connected to a Keithley 228A voltage/current source. The powders were filled into the capillary and compressed by the copper

electrodes as shown in Scheme 1. The calculated conductivity data is given in Table 2. Figure 7 shows the obtained conductivity data for the synthesized CNS-*rpc*-2h and the annealed samples. It is important to note that the conductivity of a carbon powder depends on different parameters such as defect sites, degree of graphitization, density, homogeneity, etc. [60]. While the conductivity increases with decreasing number of defects and higher graphitization, changes in powder density will significantly influence the overall conductivity of the powder [60,61].



**Scheme 1:** The set up for bulk conductivity measurement

**Table 2**. Resistance values of the synthesized CNS-*rpc*-2h annealed at 1400~2000 °C

Resistance (ohm)	Min	Max	Average
CNS-rpc-2h (raw)	5.79	7.51	6.65
CNS-ann-1400 (1400 °C)	5.12	5.48	5.30
CNS-ann-1600 (1600 °C)	3.89	4.90	4.39
CNS-ann-1800 (1800 °C)	3.83	4.87	4.35
CNS-ann-2000 (2000 °C)	6.15	7.49	6.82
Arkema multiwalled	5.31	6.01	5.66
CNT*			

<sup>\*</sup>CNT values are given for comparison only.

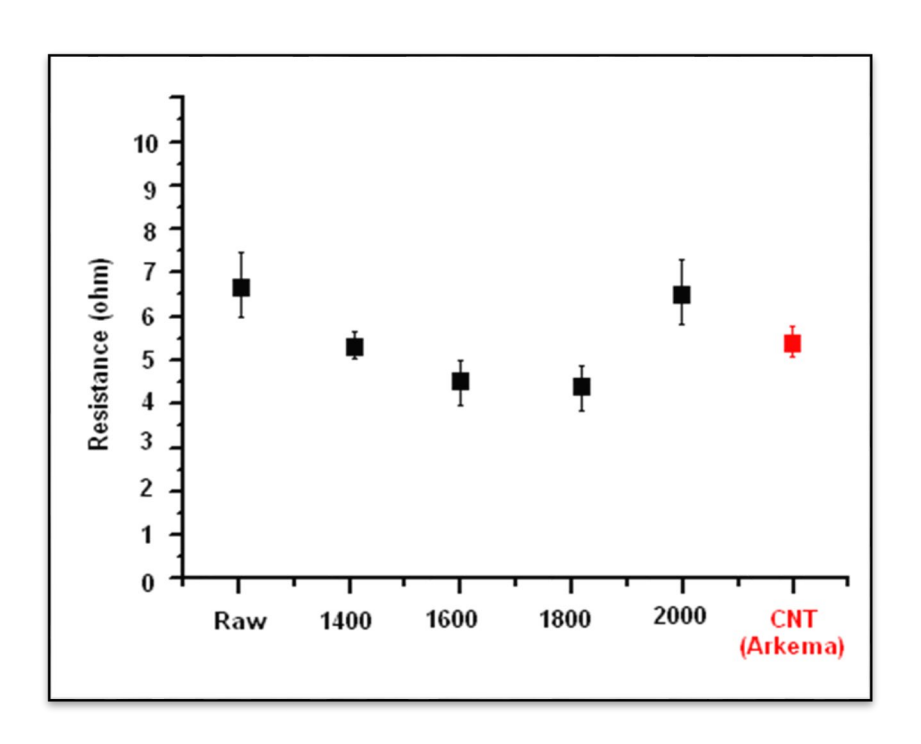


Figure 7: Plot of the resistance values for the synthesized CNS-rpc-2h annealed at 1400~2000°C

As can be seen from Fig. 7, the values of the resistance measured in the synthesized CNS-*rpc*-2h, the annealed samples at 1400~2000 °C and the Arkema multiwalled CNT are in the same range, which also fall to the same range as that for the CNS-*st* [15,16]. The annealing of the samples induces little change in the electrical conductivity. This property is supported by the Raman results that show little change in the G band or the graphitic structure. These results together prove that the CNS samples synthesized using the rapid pyrolytic carbonization process is sufficiently graphitized and has electrical properties similar to the multiwalled nanotubes. Thus, CNS may be used as electrode catalyst support and in some graphitic carbon required applications. Compared to planar graphite, less swelling is expected for CNS. Therefore, it may be of important for electrochemical applications or nuclear applications. The main effect of annealing is expected to be the passivation of the CNS surface [62].

#### 3.2.4 BET surface area and pore volume

The pore structure of the synthesized CNS-*rpc*-2h and the annealed samples at 1400~2000 °C were characterized by N<sub>2</sub> adsorption/desorption isotherms. According to the International Union of Pure and Applied Chemistry (IUPAC) nomenclature, the CNS-*rpc*-2h and the annealed samples exhibit type IV isotherms with a H<sub>2</sub>-type hysteresis [63], which indicates the formation of materials with mesopores. The BET surface area and pore volume analysis for the synthesized CNS-*rpc*-2h and the annealed samples at 1400~2000 °C are shown in Table 3. As the temperature was increased from 1000 °C to 2000 °C, the surface area and pore volume decreased when compared to the CNS synthesized using the standard method (CNS-*st*) and the MWCNT (Arkema), indicating that high temperature might convert the amorphous carbon to graphic carbon causing the reduced surface area and also collapse the pore structure causing the reduced pore volume.

**Table 3.** BET surface area and pore analysis for synthesized CNS

sample	BET surface area	Pore volume
	$(m^2/g)$	$(cm^3/g)$
CNS-rpc-2h (raw)	180	0.40
CNS-ann-1400 (1400 °C)	152	0.38
CNS-ann-1600 (1600 °C)	100	0.37
CNS-ann-1800 (1800 °C)	96	0.35
CNS-ann-2000 (2000 °C)	88	0.34
CNS-st	270	0.42
MWCNT (Arkema)	249	0.48

#### 4. Conclusion

Hollow graphitic CNS with reduced degree of inter-particle agglomeration was synthesized using rapid heating during the carbonization process when compared to the CNS synthesized using the standard slow heating. The reduced agglomeration of CNSs indicates that rapid heating effectively

mitigated the agglomeration in the formation of CNS due to rapid pyrolytic fragmentation of the crosslinked polymer precursor. The TEM, SEM, BET, XRD, bulk conductivity and Raman spectroscopy measurements demonstrated the formation of robust and less agglomerated hollow graphitic nanospheres with a significantly decreased BET surface area than that for CNS synthesized using the standard method. More importantly, this rapid pyrolytic carbonatization approach will provide important insight for future design of carbonization process to obtain carbon nanostructured materials with less degree of agglomeration.

### Acknowledgements

The authors gratefully acknowledge the financial support from Long Island University (Post) Faculty Research Grant and Undergraduate Research Grant. Support from the National Science Foundation (FAIN-1955521) is gratefully acknowledged.

#### References

- P. Karna, M. Ghimire, S. Mishra, S. Karna, Synthesis and characterization of carbon nanospheres,
   Open Access Library Journal 4 (2007) e3619
- 2. M.S. Mauter and M. Elimelech, Environmental Applications of Carbon-Based Nanomaterials, Environ. Sci. Technol. 42 (2008) 5843-5859.
- 3. J. Wen, Y. Xu, H. Li, A. Lu, S. Sun, Recent applications of carbon nanomaterials in fluorescence biosensing and bioimaging. Chem. Commun. 51 (2015) 11346-11358.
- 4. T. Chen and L. Dai, Carbon nanomaterials for high-performance supercapacitors, Mater. Today 16 (2013) 272-280.
- 5. H.W. Kroto, J.R. Heath, S.C. O'Brien, R.F. Carl, R.E. Smalley, C60: Buckminster fullerene, Nature 318 (1985) 6042 162-163.
- 6. S. Novoselov, A.K. Geim, S.V. Morozov, D. Jiang, M.I. Katsnelson, I.V. Grigorieva, S.V. Dubonos, A.A. Firsov: Two-dimensional gas of massless Dirac fermions in graphene, Nature 438 (2005) 197-200.
- 7. J. Heiligtag, M. Niederberger, The fascinating world of nanoparticle research, Mater Today 16 (2013) 262–271.
- 8. X.X. Wang, Z.H. Tan, M. Zeng, J.N. Wang: Carbon nanocages, A new support material for Pt catalyst with remarkably high durability, Sci. Rep. 4 (2014) 1-11.
- 9. Y. Chen, Y.L. Guo, P. Han, D. Li, X. Gui, Z.F. Zhang, K. Fu, M.Q, Graphitic carbon nanocages as new photothermal agent and drug Carrier for 980 nm laser driven cancer therapy, Carbon 136 (2018) 234-247.
- 10. M. Adam, A. Hart, L.A. Stevens, J. Wood, J.P. Robinson, S.P. Rigby, Microwave synthesis of carbon onions in fractal aggregates using heavy oil as a precursor, Carbon 138 (2018) 427-435.
- 11. W.B. Xu, B. Mu, and A.Q. Wang, Porous carbon nanoflakes with a high specific surface area derived from a kapok fiber for high-performance electrode materials of supercapacitors, RSC Adv. **6** (2016) 6967-6977.

- Y.S. Yun, S.Y. Cho, J. Shim, B.H. Kim, S.J. Chang, S.J. Baek, Y.S. Huh, Y. Tak, Y.W. Park,
   S. Park, H.J. Jin, Microporous carbon nanoplates from regenerated silk proteins for supercapacitors, Adv Mater. 25 (2013) 1993-1998.
- L. Fang, Y.P. Xie, Y.Y. Wang, Z.W. Zhang, P.F. Liu, N. Cheng, J.F. Liu, Y.C. Tu, H.B.
   Zhao, J.J. Zhang, Facile synthesis of hierarchical porous carbon nanorods for supercapacitors application, Appl. Surf. Sci. 464 (2019) 479-487.
- 14. X.J. He, F.H. Wu, M.D. Zheng, The synthesis of carbon nanoballs and its electrochemical performance, Diam. Relat. Mater. 16 (2007) 311-315.
- C. Zhang, G. Bhargava, M.D. Elwell, P. Parasher, B. Zhou, D. Yates, I. Knoke, I. Neitzel,
   Y. Gogotsi, Hollow graphitic carbon nanospheres: synthesis and properties. J. Mater. Sci. 49
   (2014) 1947-1956.
- 16. C. Zhang, Q.S. Gao, B. Zhou, G. Bhargava, Preparation, characterization, and surface conductivity of nanocomposites with hollow graphitic carbon nanospheres as fillers in polymethylmethacrylate matrix, J. Nanopart. Res. **19** (2017) 269.
- S. Yallappa, S.R. Kumar, K.L. Nagashree, M. Bhargavi, C.N. Rakshitha, D. Aneetta, M.P. Abhinethri, G. Hegde, Fabrication of carbon nanospheres using natural resources and their voltametric studies of dopamine, Mater. Today 5 (2018) 3093-3098.
- 18. K. Pan, H. Ming, Y. Liu, and Z. Kang, Large Scale Synthesis of Carbon Nanospheres and their Application as Electrode Materials for Heavy Metal Ions Detection, New J. Chem. 36 (2012), 113-118.
- 19. X. Sun, and Y. Li, Colloidal Carbon Spheres and Their Core/Shell Structures with Noble-Metal Nanoparticles, Angew. Chem. Int. Ed. 43 (2004) 597-601.
- A. Deshmukh, S. Mhlanga and N. Coville, Carbon Spheres, Mater. Sci. Eng. R Rep. 70 (2010)
   1-28.
- L. Qu, H. Zhang, J. Zhu, and L. Dai, Tunable Assembly of Carbon Nanospheres on Single-Walled Carbon Nanotubes, Nat. Nanotechnol. 21 (2010) 30.

- 22. X.S. Tao, Q. Zhang, Y. Li, X.L. Lv, D.L. Ma, H.G. Wang, P, S tri-doped hollow carbon nanosphere as a high-efficient bifunctional oxygen electrocatalyst for rechargeable Zn-air batteries, Appl. Surf. Sci. 490 (2019) 47–55.
- 23. H.G. Wang, Y.H. Wang, Y.H. Li, Y.C. Wan, Q. Duan, Exceptional electrochemical performance of nitrogen-doped porous carbon for lithium storage, Carbon 82 (2015) 116-123.
- 24. E. Auer, A. Freund, J. Pietsch, T. Tacke, Carbons as supports for industrial precious metal catalysts, Appl. Catal. A 173 (1998) 259-271.
- 25. J.S. Han, D.Y. Chung, D.G. Ha, J.H. Kim, K. Choi, Y.E Sung, S.H. Kang, Nitrogen and boron co-doped hollow carbon catalyst for the oxygen reduction reaction. Carbon 105 (2016) 1-7.
- 26. X. Huang, S. Wu, X. Du, Gated mesoporous carbon nanoparticles as drug delivery system for stimuli-responsive controlled release, Carbon 101 (2016) 135-142.
- A. Hirata, A. Igarashi, T. Kaito, Study on solid lubricant properties of carbon onions produced by heat treatment of diamond clusters or particles, Tribol. Int. 37 (2004) 899-905.
- 28. C. Zhang, Q.S. Gao, B. Zhou, G. Bhargava, Preparation, characterization and surface conductivity of nanocomposites with hollow graphitic carbon nanospheres as fillers in polymethylmethacrylate matrix, J. Nanopart. Res. 19 (2017) 269.
- 29. A. Draoui, M. Zidour, A. Tounsi, B. Adim, Static and dynamic behavior of nanotubes-reinforced sandwich plates using (FSDT). J. Nano. R. 57 (2019) 117-35.
- 30. M. Medani, A. Benahmed, M. Zidour, H. Heireche, A. Tounsi, A.A. Bousahla, Static and dynamic behavior of (FG-CNT) reinforced porous sandwich plate using energy principle. Steel and Composite Structures 32 (2019) 595–610. https://doi.org/10.12989/scs.2019.32.5.595
- 31. M. Hussain, M. N. Naeem, A. Tounsi, and M. Taj, Nonlocal effect on the vibration of armchair and zigzag SWCNTs with bending rigidity, Advances in nano research 7 (2019) 431-442. https://doi.org/10.12989/anr.2019.7.6.431

- 32. A. Bousahla, F. Bourada, S. R. Mahmoud, A. Tounsi, A. Algarni, E. A. A. Bedia, A. Tounsi, Buckling and dynamic behavior of the simply supported CNT-RC beams using an integral-first shear deformation theory. Computers and Concrete 25 (2020) 155-166. https://doi.org/10.12989/CAC.2020.25.2.155
- S. Asghar, M. N. Naeem, M. Hussain, M. Taj, and A. Tounsi, Prediction and assessment of nonlocal natural frequencies of DWCNTs: Vibration analysis. Computers and Concrete 25 (2020) 133-144. <a href="https://doi.org/10.12989/cac.2020.25.2.133">https://doi.org/10.12989/cac.2020.25.2.133</a>
- 34. M. Bellal, H. Hebali, H. Heireche, A.A. Bousahla, A. Tounsi, F. Bourada, Buckling behavior of a single-layered graphene sheet resting on viscoelastic medium via nonlocal four-unknown integral model. Steel and Composite Structures 35 (2020) 643-655. https://doi.org/10.12989/SCS.2020.34.5.643
- 35. F. Bourada, A.A. Bousahla, A. Tounsi, E.A.A. Bedia, S.R. Mahmoud, K.H. Benrahou, Stability and dynamic analyses of SW-CNT reinforced concrete beam resting on elastic-foundation. Computers and Concrete 25 (2020) 485-495. <a href="https://doi.org/10.12989/CAC.2020.25.6.485">https://doi.org/10.12989/CAC.2020.25.6.485</a>
- 36. N. Bendenia, M. Zidour, A.A. Bousahla, F. Bourada, A. Tounsi, K.H. Benrahou, Deflections, stresses and free vibration studies of FG-CNT reinforced sandwich plates resting on Pasternak elastic foundation. Computers and Concrete 26 (2020) 213-226. https://doi.org/10.12989/CAC.2020.26.3.213
- 37. F. Khosravi, S.A. Hosseini, A. Tounsi, Forced axial vibration of a single-walled carbon nanotube embedded in elastic medium under various moving forces. J. Nano. R. 63 (2020) 112–33. https://doi.org/10.4028/www.scientific.net/jnanor.63.112.
- 38. A.B. Fuertes and S. Alvarez, Graphitic mesoporous carbons synthesized through mesostructured silica templates, Carbon 42 (2004) 3049-3055.
- 39. W.M. Qiao, J. Song, S.Y. Lim, S.H. Hong, S.H. Yoon, I. Mochida, T. Imaoka, Carbon nanospheres produced in an arc-discharge process, Carbon 44 (2006) 187-190.

- 40. T.C. Liu and Y.Y Li, Synthesis of carbon nanocapsules and carbon nanotubes by an acetylene flame method, Carbon 44 (2006) 2045-2050.
- 41. A.M. Herring, J.T. Mckinnon, B.D. McClosky, J. Filley, K.W. Gneshin, R.A. Pavelka, A novel method for the templated synthesis of homogeneous samples of hollow carbon nanospheres from cellulose chars. J. Am. Chem. Soc. 125 (2003) 9916.
- 42. G. Hu, D. Ma, M. Cheng, L. Liu, X. Bao, Direct synthesis of uniform hollow carbon spheres by a self-assembly template approach, Chem. Commun. 17 (2002) 1948-1949.
- 43. J.M. Du and D.J. Kang, Synthesis of carbon nanostructures with unique morphologies via a reduction-catalysis reaction route, Mater. Res. Bull. 41 (2006) 1785-1790.
- 44. J.W. Liu, M.W. Shao, Q. Tang, X.Y. Cheng, Z.P. Liu, Y.T Qian, A medial-reduction route to hollow carbon spheres, Carbon 41 (2003) 1682-1685.
- 45. N.A. Katcho, E. Urones-Garrote, D. Avila-Brande, A. Gomez-Herrero, S. Urbonaite, S. Csillag, Carbon Hollow Nanospheres from Chlorination of Ferrocene, Chem. Mater. **19** (2007) 2304-2309.
- 46. Z. Li, M. Jaroniec, Y. Lee, L.R. Radovic, High surface area graphitized carbon with uniform mesopores synthesized by a colloidal imprinting method, Chem. Commun. **13** (2002) 1346-1347.
- 47. R. Atif and F. Inam, Reasons and remedies for the agglomeration of multilayered graphene and carbon nanotubes in polymers, in: Sidorenko AS (ed) Physics, chemistry and biology of functional nanostructures III, Beilstein, 2016, pp.1174-1196.
- 48. D.L. Shi, X. Feng, Y.Y. Huang, K.C. Hwang, H.J. Gao, The effect of nanotube waviness and agglomeration on the elastic property of carbon nanotube- reinforced composites. J. Eng. Technol. 126 (2004) 250-257.
- 49. M.J. Sobkowicza, J.R. Dorgana, K.W. Gneshinb, A.M. Herringa, J.T. McKinnona, Controlled dispersion of carbon nanospheres through surface functionalization, Carbon 47 (2009) 622-628.
- 50. H. Wang, W. Zhou, D.L. Ho, K.I. Winey, J.E. Fischer, C.J. Glinka, E.K. Hobbie, Dispersing single-walled carbon nanotubes with surfactants: a small angle neutron scattering study, Nano.

- Lett. 4 (2004) 1789-1793.
- 51. C. Deeney, E.P. McKiernan, S.A. Belhout, B.J. Rodriguez, G. Redmond, S.J. Quinn, Template-assisted synthesis of luminescent carbon nanofibers from beverage-related precursors by microwave heating, Molecules 24 (2019) 1455.
- 52. T. Kim, J. Lee, K.H. Lee, Microwave heating of carbon-based solid materials, Carbon Lett. **15** (2014) 15-24.
- 53. J.A. Menéndez, A. Arenillas, B. Fidalgo, Y. Fernández, L. Zubizarreta, E.G. Calvo, J.M. Bermúdez, Microwave heating processes involving carbon materials, Fuel Process. Technol. **91** (2010) 1–8.
- 54. Q.G. Yan, H. Toghiani, Z.Y. Cai, J.L. Zhang, Formation of nanocarbon spheres by thermal treatment of wood char from fast pyrolysis process, Wood Fiber Sci. **46** (2013) 437-450.
- 55. J. Prekodravac, Z. Marković, S. Jovanović, M. Budimir, D. Peruško, I., Holclajtner-Antunović, V. Z. Pavlović Syrgiannis, A. Bonasera, B. Todorović-Marković, The effect of annealing temperature and time on synthesis of graphene thin films by rapid thermal annealing, Synth. Met. 209 (2015) 461-467.
- 56. Y. Yao, F. Chen, A. Nie, S.D. Lacey, R.J. Jacob, S. Xu, Z. Huang, K. Fu, J. Dai, L. Salamanca-Riba, M.R. Zachariah, R. Shahbazian-Yassar, L. Hu, In Situ High Temperature Synthesis of Single-Component Metallic Nanoparticles, ACS Cent. Sci. 3 (2017) 294-301.
- 57. L.S. Roselin, R.S. Juang, C.T. Hsieh, S. Sagadevan, A. Umar, R. Rosilda Selvin and H.H. Hegazy, Recent Advances and Perspectives of Carbon-Based Nanostructures as Anode Materials for Li-ion Batteries, Materials 12 (2019) 1229.
- 58. C. Vix-Guterl, M. Couzi, J. Dentzer, M. Trinquecoste, P. Delhaes, Surface Characterizations of Carbon Multiwall Nanotubes: Comparison between Surface Active Sites and Raman Spectroscopy, J. Phys. Chem. B 108 (2004) 19361-19367.
- 59. P.H. Tan, S. Dimovski, Y. Gogotsi, Raman scattering of non-planar graphite, arched edges, polyhedral crystals, whiskers and cones, Philos. Trans. A Math Phys. Eng. Sci. **362** (2004) 2289-

2310.

- 60. A. Celzard, J.F. Marêché, F. Payot, G. Furdin, Electrical conductivity of carbonaceous powders, Carbon 40 (2002) 2801-2815.
- 61. B. Marinho, M. Ghislandi, E. Tkalyac, C.E. Koning, Electrical conductivity of compacts of graphene, multi-wall carbon nanotubes, carbon black, and graphite powder, Powder Technol. 221 (2012) 351-358.
- 62. H. Jin, Y. Kwang-sun, J. Junghoon, C. Heon, M. Lee, Annealing effect on surface passivation of a-Si:H/c-Si interface in terms of crystalline volume fraction, Curr. Appl. Phys. **10** (2010) 5375-5378.
- 63. S. Fujii, H. Tsuchida, M. Koʻmoto, Chemical studies on the reaction products of glucose and ammonia, Part X. Isolation and identification of 4 (5)- (DL-Glycero-2,3-Dihydroxypropyl)

  Imidazole, Agr. Biol. Chem. 30 (1966) 73-77.